COBEM 2023 27TH INTERNATIONAL CONGRESS OF MECHANICAL ENGENEERING

ABCM Brazilian Society of Mechanical Sciences and Engineering
27th ABCM International Congress of Mechanical Engineering
December 04-08, 2023, Florianópolis-SC, Brazil

COB-2023-0943
NUMERICAL ANALYSIS OF THE LIQUID FILM THICKNESS FOR GAS-LIQUID FLOWS ON THE SEPARATED PATTERN: CLOSING PARAMETERS INFLUENCE

Elen Louise Camargo Cominesi*
Vinícius Valenga†
Alysson Henrique Rublesperger de Almeida‡
Victor Vaurek Dimbarre§
Luiz Eduardo Melo Lima¶

Department of Mechanics, Federal University of Technology—Paraná—, Ponta Grossa, PR 84017-220, Brazil

*elencominesi@alunos.utfpr.edu.br, †vinivalenga@gmail.com, ‡alyssonhra99@gmail.com, §victorv_dimbarre@hotmail.com, ¶lelima@utfpr.edu.br

Abstract. *The separated flow is a two-phase flow pattern in ducts constituted by two sub-patterns, stratified and annular. These two sub-patterns present a thin liquid film in contact with the pipe wall and a gas core that drags liquid droplets from the film. Experimentally determining the liquid film thickness is a challenging task with high limitations. Therefore, mathematical models based on the physical aspects of the phenomenon are developed and employed to estimate the liquid film thickness. Several parameters are essential for closing these models, including the entrainment fraction of the droplets and the interfacial friction factor, which are often modeled through empirical correlations. This work evaluated the influence of the entrainment fraction of the droplets and the interfacial friction factor on the film thickness prediction using various empirical correlations. For this purpose, a computational code was developed to solve the implicit equation of the film model. The results obtained for the film thickness were compared with experimental databases from the literature for horizontal stratified and vertical annular flow. The combination of both correlations that produces the best results from the obtained deviations was identified.*

Keywords: *multiphase flow, liquid film thickness, modeling.*

1. INTRODUCTION

Multiphase flow is the simultaneous transport of distinct fluid phases within the same pipeline. Gas-liquid flow is an example of two-phase flow, where various phase distributions can be observed along the pipe. This flow is encountered in numerous industrial applications, such as heat exchangers, condensers, distillation towers, and chemical reactors. The flow pattern followed by the liquid and gas phases depends on the forces acting on the fluids, phase flow rates, pipe geometric characteristics, and physical properties of the phases. The separated flow is a pattern that can be sub-classified into stratified and annular flow. In annular flow, the liquid flows as a film along the pipe wall, while a gas core flows in the center, carrying an amount of liquid as droplets (Sawant *et al.*, 2008). Higher gas flow rates in annular flows result in a wide dispersion of liquid in the core and a thinner liquid film on the wall. A semi-annular flow can be observed with a low gas flow rate, where a significant portion of the liquid flows at the bottom of the pipe. At the same time, unstable waves are dragged around the pipe, occasionally touching the upper part. In the stratified pattern observed in horizontal flows, the liquid and the gas phases are separated by gravity, with the liquid film flowing only in the lower portion of the pipe. In contrast, the gas core flows in the upper portion. The stratified pattern can be categorized as smooth and wavy according to the interface shape (Shoham, 2006).

The study of liquid film characteristics provides essential information regarding erosion, corrosion, and heat transfer aspects in the pipelines of the previously mentioned industrial applications. Several researchers have focused on determining the film thickness and the dominant factors influencing its formation. Fukano and Ousaka (1989) developed a satisfactory model to determine the mechanism responsible for liquid film formation and calculate its circumferential distribution in air-water two-phase flows in horizontal and semi-horizontal pipes. At relatively low gas velocities, the interface between phases is quite stable. However, as the gas velocity increases, waves appear at the interface due to the instability caused by this increase, resulting in shear forces exceeding the surface tension, leading to the entrainment of droplets. Their investigation concluded that the liquid retained in the perturbation waves replenishes the gravity-drained liquid film due to the increased static pressure resulting from the gas flow stagnation immediately behind the wave. Besides being the major contributors to the entrainment of droplets, these perturbation waves crossing the liquid film interface act as roughness for the central gas flow and significantly contribute to pressure drop due to friction (Sawant *et al.*, 2008).

Pedras (1993) observed that the momentum transfer from gas to the liquid film in annular flow occurs predominantly at the interface due to interfacial tension. However, for flows with relatively thick films, the interfacial tension is combined and superimposed with the action of gravity. The gas flow significantly influences interfacial tension, which increases with the increased gas velocity due to a decrease in film thickness and wave frequencies propagating through it. The entrainment of droplets is directly related to the interfacial shear, as the droplets dispersed in the gas core are formed by the liquid detaching from the liquid film wave crests. The redeposition of droplets into the liquid film after leaving the core can considerably increase the wall shear stress. Furthermore, higher gas superficial velocities lead to smaller entrained droplets, with these being the first to be redeposited when the core has high velocity.

Seshadri *et al.* (2014) studied the formation and thickness of liquid films in two-phase flows in pipes of different diameters. In their research, they observed that the formation of the film is based on the viscosity characteristics at the interface between the phases. However, the magnitude of the liquid film thickness is influenced by factors such as surface tensions, body or inertial forces, the superficial velocities of the phases, and the dimensions of the pipe in which the flow occurs. They assert that in conventional flows, gravity is the dominant factor determining the film thickness, while in smaller-diameter pipes, surface tension governs the behavior and thickness of the film.

This study aims to determine the thickness of the liquid film in gas-liquid flows in the separated pattern. For this purpose, a computational code was developed in MATLAB® language to analyze the relevant parameters of film formation. Some of the correlations available in the literature for entrainment fraction of droplets and interfacial friction factor were employed in the developed code. The results were compared with experimental data found in the literature regarding annular and stratified flows.

2. MODEL

The gas-liquid flow in the separated pattern consists of two distinct (continuous) phases or components that flow concurrently, separated by a well-defined interface. In stratified flow, the liquid phase ($_l$) flows in the lower portion of the pipe as a flat film ($_f$), while the gas phase ($_g$) flows in the upper portion as a core ($_c$). The interface ($_i$) is generally smooth in horizontal or nearly horizontal flow at low velocities. However, as the inclination or superficial gas velocity increases, the interface becomes wavy, and the liquid film adheres to the pipe walls. Beyond this point, any increase in the superficial gas velocity can lead to film closure, forming an annular flow. The gas core may contain liquid droplets ($_d$) resulting from atomization and deposition processes (Shoham, 2006). The numerical model is based on the works developed by Taitel and Dukler (1976) and Alves *et al.* (1991) and considers a separated flow flowing in a pipe of diameter D, perimeter S, cross-sectional area A, absolute roughness ϵ, and inclination θ, under a gravitational field of acceleration g. The model for determining the dimensionless film thickness ($\delta_f \equiv H_f/D$, where H_f is the film thickness) is obtained from the momentum conservation equations for both the gas core and the liquid film, subtracting the equation for the gas core from the equation for the liquid film and eliminating the pressure gradient:

$$f(\delta_f) = \frac{\tau_c S_c}{A_c} - \frac{\tau_f S_f}{A_f} + \tau_i S_i \left(\frac{1}{A_c} + \frac{1}{A_f}\right) - (\rho_f - \rho_c)\, g \sin\theta = 0 \tag{1}$$

The wall shear stress of a phase (or region) k, e.g., core ($k = c$) and film ($k = f$), is defined in terms of the Fanning friction factor, C_{fk}, as follows:

$$\tau_k = \frac{1}{2} C_{fk} \rho_k U_k \left|U_k\right| \tag{2}$$

and C_{fk} can be determined using the Hagen-Poiseuille law for laminar flow or the (explicit) correlation by Haaland (1983) for turbulent flow, among others, according to Eq. (3):

$$C_{fk} = \begin{cases} \frac{16}{\mathrm{Re}_k} & \text{if laminar} \\ \left\{-3.6 \log\left[\left(\frac{\epsilon}{3.7 D_k}\right)^{1.11} + \frac{6.9}{\mathrm{Re}_k}\right]\right\}^{-2} & \text{if turbulent} \end{cases} \tag{3}$$

where the Reynolds number, Re_k, is defined in terms of the local velocity, hydraulic diameter, and kinematic viscosity, U_k, D_k, and ν_k, respectively, of a phase (or region) k as:

$$\mathrm{Re}_k = U_k D_k / \nu_k \tag{4}$$

The interfacial shear stress, τ_i, can also be defined by a similar expression as presented in Eq. (2), considering the relative velocity, $V_r = U_c - U_f$, the gas core density, ρ_c, and the interfacial friction factor, C_{fi}:

$$\tau_i = \frac{1}{2} C_{fi} \rho_c V_r \left|V_r\right| \tag{5}$$

In the separated pattern, the gas core flows at a much higher velocity, U_c, than the liquid film velocity, U_f. Equations (6) and (7) define U_c and U_f based on the gas and liquid superficial velocities, J_g and J_l, core and film area fractions, ϕ_c and ϕ_f, and entrainment fraction of droplets, E_d.

$$U_c = \left(J_g + E_d J_l\right)/\phi_c \tag{6}$$

$$U_f = \left(J_l - E_d J_l\right)/\phi_f \tag{7}$$

The interface kind, whether flat or concentric, determines the geometric properties of the phases (or regions), such as the interface angle, λ_i, area fractions, ϕ_f and ϕ_c, wetted perimeters, S_f and S_c, interfacial perimeter, S_i, cross-sectional areas, A_f and A_c, and hydraulic diameters, D_f and D_c, as shown in Tab. 1.

Table 1. Equations for the geometric properties of separated flow according to the interface shape.

Geometric	Interface shape	
property	Flat $(0 < \delta_f < 1)$	Concentric $(0 < \delta_f < 0.5)$
λ_i	$2\arccos\left(1-\delta_f\right)$	2π
ϕ_f	$\left(\lambda_i - \sin\lambda_i\right)/\left(2\pi\right)$	$4\delta_f\left(1-\delta_f\right)$
ϕ_c	$1-\phi_f$	(1)
S_f	$\lambda_i/\left(2\pi\right)$	S
S_c	$S - S_f$	0
S_i	$S\sin\left(\lambda_i/2\right)/\pi$	$S\left(1-2\delta_f\right)$
A_f	$\phi_f A$	(1)
A_c	$\phi_c A$	(1)
D_f	$4A_f/S_f$	(1)
D_c	$4A_c/\left(S_c+S_i\right)$	(1)

(1) Equal to that of the flat interface.

The film density and dynamic viscosity correspond to the liquid, such that $\rho_f = \rho_l$ and $\mu_f = \mu_l$. The density and dynamic viscosity of the core are defined as:

$$\rho_c = \phi_{gc}\rho_g + \phi_d\rho_l \tag{8}$$

$$\mu_c = \phi_{gc}\mu_g + \phi_d\mu_l \tag{9}$$

In the core region, the gas area fraction, ϕ_{gc}, is obtained from the droplets' area fraction, $\phi_{gc} = 1 - \phi_d$. The droplets' area fraction, ϕ_d, is defined as a function of the entrainment fraction of droplets, E_d, and the superficial velocities of the gas and liquid phases, J_g and J_l:

$$\phi_d = \frac{J_l E_d}{J_g + J_l E_d} \tag{10}$$

2.1 Entrainment fraction correlations

The droplets' atomization and deposition rates are similar under steady-state conditions and far from the film formation region, resulting in a locally uniform entrainment fraction of droplets. This fraction can be estimated using simplified physical models or empirical correlations from the literature. However, these correlations suffer from the imprecision of experimental data and the absence of a consistent physical model to represent them. The correlations to estimate droplets' entrainment fraction typically consider the pipe characteristics, properties of the fluids, and superficial velocities of the phases. These correlations are often presented in terms of dimensionless numbers. Table 2 shows ten correlations for the entrainment fraction of droplets selected from the literature for further analysis in the present work.

The maximum entrainment fraction of droplets, $E_{d\max}$, is given by:

$$E_{d\max} = 1 - \frac{\mathrm{Re}_{l\mathrm{crit}}}{\mathrm{Re}_l} \tag{11}$$

where the critical liquid Reynolds number, $\mathrm{Re}_{l\mathrm{crit}}$, is calculated according to the correlation employed (Tab. 2):

$$\mathrm{Re}_{l\mathrm{crit}} = \begin{cases} 0 & \text{if CE1, CE2, CE3, and CF5} \\ \exp\left(5.80405 + \frac{0.4249}{\omega}\right) & \text{if CE4} \\ 7.3(\log\omega)^3 + 44.2(\log\omega)^2 - 236(\log\omega) + 439 & \text{if CE6, CE7, and CE10} \\ 250\ln\mathrm{Re}_l - 1265 & \text{if CE8} \\ \frac{13}{\sqrt{N_\mu}} + 0.3\left(\mathrm{Re}_l - \frac{13}{\sqrt{N_\mu}}\right)^{0.95} & \text{if CE9} \end{cases} \tag{12}$$

Table 2. Correlations for the entrainment fraction of droplets E_d.

Correlation	$E_d/E_{d\max}$	Author
CE1	$0.015 + 0.44 \log\left[10^4 \frac{\rho_c}{\rho_l}\left(\frac{J_g \mu_l}{\sigma}\right)^2\right]$	Paleev and Filippovich (1966)
CE2	$1 - \exp\left[-0.125\left(10^4 \frac{\mathrm{We}_g}{\mathrm{Re}_g}\sqrt{\frac{\rho_g}{\rho_l}} - 1.5\right)\right]$	Wallis (1968)
CE3	$\frac{\Omega}{1+\Omega}$	Oliemans *et al.* (1986)
CE4	$\begin{cases} \exp\left(-6.8872 + 0.472 \ln I_m\right) & \text{if } I_m \times 10^{-6} < 1.35 \\ 0.69 + 8.03 \times 10^{-8} I_m & \text{if } 1.35 \leq I_m \times 10^{-6} \leq 2.15 \\ \exp\left(-1.775 + 0.112 \ln I_m\right) & \text{if } I_m \times 10^{-6} > 2.15 \end{cases}$	Owen (1986)
CE5	$\tanh\left(7.25 \times 10^{-7} I_m\right)$	Ishii and Mishima (1989)
CE6	$\frac{\Omega}{1+\Omega}$	Pan and Hanratty (2002a)
CE7	$\frac{\Omega}{1+\Omega}$	Pan and Hanratty (2002b)
CE8	$\tanh\left(2.31 \times 10^{-4} \mathrm{Re}_l^{-0.35} \widetilde{\mathrm{We}}_g^{\,5/4}\right)$	Sawant *et al.* (2008)
CE9	$\tanh\left(2.31 \times 10^{-4} \mathrm{Re}_l^{-0.35} \widetilde{\mathrm{We}}_g^{\,5/4}\right)$	Sawant *et al.* (2009)
CE10	$\frac{\Omega}{1+\Omega}$	Karami *et al.* (2017)

The liquid Reynolds number, Re_l, is calculated using Eq. (4), but considering the liquid superficial velocity, J_l, pipe diameter, D, and liquid kinematic viscosity, ν_l. Analogously, this can be done for the gas Reynolds number, Re_g (CE2). Furthermore, the dimensionless group of physical properties is expressed as $\omega = (\mu_l/\mu_g)\sqrt{\rho_g/\rho_l}$ (Asali, 1984), and the (dimensionless) viscosity number, N_μ, is defined as a function of the Morton number, Mo:

$$N_\mu = \mu_l \left(\frac{g\Delta\rho}{\rho_l^2 \sigma^3}\right)^{1/4} \equiv (\mathrm{Mo})^{1/4} \tag{13}$$

where $\Delta\rho = \rho_l - \rho_g$ is the density difference, and σ is the gas-liquid surface tension.

The gas Weber number, We_g (CE2), and modified gas Weber numbers, $\widehat{\mathrm{We}}_g$ (CE5) and $\widetilde{\mathrm{We}}_g$ (CE8 and CE9), are defined as:

$$\mathrm{We}_g = J_g^2 D \rho_g / \sigma \tag{14}$$

$$\widehat{\mathrm{We}}_g = \mathrm{We}_g \left(\frac{\Delta\rho}{\rho_g}\right)^{1/3} \tag{15}$$

$$\widetilde{\mathrm{We}}_g = \mathrm{We}_g \left(\frac{\Delta\rho}{\rho_g}\right)^{1/4} \tag{16}$$

The dimensionless group I_m (CE4 and CE5) is given by:

$$I_m = \mathrm{Re}_l^{1/4} \widehat{\mathrm{We}}_g^{\,5/4} \tag{17}$$

and the dimensionless group Ω is calculated according to the correlation employed (Tab. 2):

$$\Omega = \begin{cases} 10^{-2.52} J_g^{1.44} J_l^{0.7} \rho_g^{0.18} \rho_l^{1.08} \mu_g^{0.28} \mu_l^{0.27} \sigma^{-1.8} g^{0.46} D^{1.72} & \text{if CE3} \\ 9 \times 10^{-8} \frac{J_g^3 D \sqrt{\rho_g \rho_l}}{\sigma} \left(\frac{\rho_g^{1-m} \mu_g^m}{g D_d^{1+m} \rho_l}\right)^{1/(2-m)} & \text{if CE6} \\ 6 \times 10^{-5} \frac{J_g^2 D \sqrt{\rho_g \rho_l}}{\sigma} & \text{if CE7} \\ 3 \times 10^{-8} \mathrm{We}_g^{5/4} \frac{J_g - J_{g\mathrm{atom}}}{U_{d\mathrm{term}}} \frac{D}{S_{\mathrm{atom}}} \sqrt{\frac{\rho_l}{\rho_g}} & \text{if CE10} \end{cases} \tag{18}$$

The exponent m depends on the Reynolds number for the droplets' (terminal) velocity, $\mathrm{Re}_{d\mathrm{term}} = U_{d\mathrm{term}} D_d / \nu_g$, according to Eq. (19):

$$m = \begin{cases} 1 & \text{if Stokes regime } \left(U_{d\mathrm{term}} = \frac{g D_d^2 \Delta\rho}{18 \mu_g}\right) : \mathrm{Re}_{d\mathrm{term}} < 2 \\ 0.6 & \text{if transition regime } \left(U_{d\mathrm{term}} = \frac{g D_d^{8/5} \Delta\rho}{13.9 \rho_g^{2/5} \mu_g^{3/5}}\right) : 2 \leq \mathrm{Re}_{d\mathrm{term}} \leq 500 \\ 0 & \text{if Newton regime } \left(U_{d\mathrm{term}} = \sqrt{\frac{1.32 g D_d \Delta\rho}{\rho_g}}\right) : \mathrm{Re}_{d\mathrm{term}} > 500 \end{cases} \tag{19}$$

The Sauter mean diameter of the droplets, D_d, is given as a function of We_g and the Bond number ($\mathrm{Bo} = gD\rho_l/\sigma$):

$$D_d = \frac{0.14}{\mathrm{We}_g\sqrt{\mathrm{Bo}}} \tag{20}$$

The gas superficial velocity at the onset of entrainment, $J_{g\mathrm{atom}}$, and atomization length, S_{atom}, are defined as:

$$S_{\mathrm{atom}} = S\left[0.62\phi_l^{0.374}\left(\frac{0.07}{\sigma}\right)^{0.15} + \frac{\mathrm{Fr}_g^{4/5}\mathrm{We}_g^{1/4}}{\cos\theta}\frac{\rho_g}{\Delta\rho}\right] \tag{21}$$

$$J_{g\mathrm{atom}} = 5\sqrt{\rho_{g\mathrm{atm}}/\rho_g} \tag{22}$$

where the (homogeneous) liquid holdup is $\phi_l = J_l/(J_g + J_l)$, the gas Froude number is $\mathrm{Fr}_g = J_g/\sqrt{gD}$, and $\rho_{g\mathrm{atm}}$ is the gas density at the standard atmospheric condition.

2.2 Interfacial friction correlations

In the literature, several studies present correlations for the interfacial friction factor, C_{fi}. Many of these correlations exhibit reasonable accuracy when applied under appropriate conditions, and their limitations are respected. This work conducts a comparative analysis considering the correlations presented in Tab. 3.

Table 3. Correlations for the interfacial friction factor C_{fi}.

Correlation	C_{fi}	Author
CF1	C_{fc}	Taitel and Dukler (1976)
CF2	$C_{fc}\left[1 + 24\delta_f\left(\frac{\rho_g}{\rho_l}\right)^{1/3}\right]$	Whalley and Hewitt (1978)
CF3	$0.008 + 2\times10^{-5}\mathrm{Re}_l$	Cheremisinoff and Davis (1979)
CF4	$0.005 + \Pi_{\mathrm{Eo1}}\left(\frac{\delta_f}{\sqrt{\mathrm{Eo}}}\right)^{\Pi_{\mathrm{Eo2}}}$	Bharathan and Wallis (1983)
CF5	$\begin{cases} 0.96\mathrm{Re}_g^{-0.52} & \text{if } \mathrm{Re}_g \le \beta \\ 7.5\times10^{-5}\phi_f^{-1/4}\mathrm{Re}_g^{-0.3}\mathrm{Re}_l^{0.83} & \text{if } \mathrm{Re}_g > \beta \end{cases}$	Kowalski (1987)
CF6	$0.0625\left[\log\left(\frac{\epsilon_i}{3.715D} + \frac{15}{\mathrm{Re}_c}\right)\right]^{-2}$	Hamersma and Hart (1987)
CF7(1)	$\begin{cases} C_{fc} & \text{if } J_g \le J_{g\mathrm{atom}} \\ C_{fc}\left[1 + 15\sqrt{\delta_f}\left(\frac{J_g}{J_{g\mathrm{atom}}} - 1\right)\right] & \text{if } J_g > J_{g\mathrm{atom}} \end{cases}$	Xiao *et al.* (1990)
CF8	$\begin{cases} C_{fc}\left(1 + 300\delta_f\right) & \text{if } E_d > 0.9 \\ C_{fc}\left[1 + 24\delta_f\left(\frac{\rho_g}{\rho_l}\right)^{1/3}\right] & \text{if } E_d \le 0.9 \end{cases}$	Kaya *et al.* (1999)
CF9	$52\left(1 - \sqrt{\phi_g}\right)\left(\frac{\rho_g}{\rho_l}\right)\mathrm{Re}_{V_{gJ}}^{2/5} - 0.0078$	Pedras (1993)
CF10(2)	$1.7\left(12 + \frac{\nu_l}{\nu_{l20^\circ\mathrm{C}}}\right)^{-1.33}\left(1 + 12\delta_f\right)^8$	Fukano and Furukawa (1998)

(1) If $D \le 0.127$ m, conversely, C_{fi} is calculated by Eq. (3), considering ϵ_i, D_c, and Re_c.
(2) $\nu_{l20^\circ\mathrm{C}}$ is the liquid kinematic viscosity at 20 °C.

The core friction factor, C_{fc}, is calculated by Eq. (3). The Eötvös number, Eo, and its two dimensionless function groups, Π_{Eo1} and Π_{Eo2}, are given in CF4 by:

$$\mathrm{Eo} = gD^2\Delta\rho/\sigma \tag{23}$$

$$\Pi_{\mathrm{Eo1}} = 10^{\frac{9.07}{\sqrt{\mathrm{Eo}}} - 0.56} \tag{24}$$

$$\Pi_{\mathrm{Eo2}} = \frac{4.74}{\sqrt{\mathrm{Eo}}} + 1.63 \tag{25}$$

The parameter β (CF5) is a function of the Eötvös and (liquid) Reynolds numbers and the kinematic viscosities of the phases:

$$\beta = 8.78\times10^3\mathrm{Eo}^{0.9}\mathrm{Re}_l^{-0.405}\left(\frac{\nu_l}{\nu_g}\right)^{0.72} \tag{26}$$

The absolute roughness of the gas-liquid interface, ϵ_i (CF6 and CF7), is defined by:

$$\epsilon_i = \begin{cases} 0.575 D \phi_f \frac{2\pi}{\lambda_i} & \text{if CF6} \\ \begin{cases} 34 \frac{\sigma}{\rho_g V_r^2} & \text{if } (N_\mu \mathrm{We}_g)_i \leq 0.005 \\ 170 \frac{\sigma (N_\mu \mathrm{We}_g)_i^{0.3}}{\rho_g V_r^2} & \text{if } (N_\mu \mathrm{We}_g)_i > 0.005 \end{cases} & \text{if CF7} \end{cases} \tag{27}$$

where $(N_\mu \mathrm{We}_g)_i = V_r^2 \mu_l^2 (\rho_g / \rho_l) / \sigma^2$ corresponds to the product of the viscosity and Weber numbers for the interface.

The gas area fraction, ϕ_g (CF9), depends on the dimensionless group Π_{Re_l}. The Reynolds number $\mathrm{Re}_{V_{gJ}}$ (CF9) is calculated by Eq. (4), considering the gas drift velocity, V_{gJ}, pipe diameter, D, and liquid kinematic viscosity, ν_l. The definitions proposed by Pedras (1993) for Π_{Re_l}, ϕ_g, and V_{gJ} are:

$$\Pi_{\mathrm{Re}_l} = 1.255 \times 10^{-3} \mathrm{Re}_l^{0.56} \frac{J_g}{J_l} \tag{28}$$

$$\phi_g = \frac{\Pi_{\mathrm{Re}_l}}{1 + \Pi_{\mathrm{Re}_l}} \tag{29}$$

$$V_{gJ} = \frac{J_g}{\Pi_{\mathrm{Re}_l}} - J_l \tag{30}$$

2.3 Solution procedure

To solve the numerical model for dimensionless film thickness estimation, Eq. (1), it is necessary to apply an iterative method for solving nonlinear equations, such as the bisection method. Equation (1) is implicit in δ_f, as its terms and some auxiliary correlations depend on the dimensionless film thickness. Therefore, in each iteration step, it is necessary to recalculate the δ_f and all related variables until the convergence criterion is achieved. The convergence criterion of the bisection method was a residual smaller than 10^{-6}. The mathematical model, all auxiliary equations and correlations, and the bisection method were implemented in a MATLAB® computational code to generate the results necessary to perform the analysis proposed in this work.

3. EXPERIMENTAL DATA

It is necessary to utilize experimentally obtained data to compare and analyze the accuracy of the numerically obtained results for film thickness in gas-liquid flows in the separated pattern. For this purpose, this study employed the data from Torres (1992) and Aliyu *et al.* (2017).

In the Torres (1992) study, the analyses were performed using air and water in a horizontal pipe with an internal diameter of 38.1 mm under pressure and temperature close to standard atmospheric conditions. The superficial air velocity ranged from 4.5 m/s to 25.0 m/s, while the water velocity ranged from 0.01 m/s to 0.07 m/s, resulting in a stratified flow pattern. Data for vertical air-water flow in the annular pattern were obtained from the study by Aliyu *et al.* (2017), using a pipe with an internal diameter of 101.6 mm and a length of 20 m. The analyses were also conducted under temperature and pressure close to atmospheric conditions. The gas and liquid superficial velocities ranged from 11 m/s to 29 m/s and from 0.1 m/s to 1 m/s, respectively. The results obtained from the studies of Torres (1992) and Aliyu *et al.* (2017) are presented in Tab. 4.

3.1 Comparison method

The accuracy of the results for δ_f is evaluated through the calculation of the mean relative deviations, $\bar{\varepsilon}$, between the numerically computed values (calc) obtained from the developed code and the experimentally measured values (meas), considering each combination of analyzed correlations of E_d and C_{fi}. The root mean square (RMS) of the relative deviations for δ_f is also calculated based on the results of N experimental tests from each dataset used. Equations (31) and (32) provide the definitions of $\bar{\varepsilon}$ and RMS, respectively:

$$\bar{\varepsilon} \equiv \frac{1}{N} \sum \varepsilon = \frac{1}{N} \sum \left| \frac{\delta_{f\mathrm{calc}} - \delta_{f\mathrm{meas}}}{\delta_{f\mathrm{meas}}} \right| \tag{31}$$

$$\mathrm{RMS} = \sqrt{\frac{\sum (\varepsilon - \bar{\varepsilon})^2}{N}} \tag{32}$$

To validate the model, Eq. (1), against experimental data and analyze the accuracy of the results for each correlation combination (E_d and C_{fi}), Eqs. (31) and (32) were also implemented in the MATLAB® computational code.

Table 4. Experimental data used to compare against the numerical model results.

Stratified flow (Torres, 1992)					Annular flow (Aliyu *et al.*, 2017)				
Test (#)	P (Pa)	J_g (m/s)	J_l (m/s)	H_f (mm)	Test (#)	$P \times 10^{-5}$ (Pa)	J_g (m/s)	J_l (m/s)	H_f (mm)
1	95039.43	4.5	0.0088	2.882	1	1.09	18.39	0.1	1.2
2	94985.29	9.3	0.0088	2.154	2	1.13	23.66	0.1	1.0
3	94647.92	12.1	0.0088	1.512	3	1.15	28.87	0.1	0.7
4	95461.93	16.8	0.0106	0.968	4	1.10	12.08	0.2	1.2
5	95845.72	20.5	0.0128	0.788	5	1.14	17.51	0.2	1.2
6	95859.04	25.1	0.0114	0.496	6	1.18	22.41	0.2	1.0
7	95439.94	4.5	0.0209	5.040	7	1.23	26.90	0.2	1.0
8	95411.31	9.3	0.0209	3.385	8	1.13	11.70	0.3	1.3
9	95532.46	12.3	0.0209	2.187	9	1.18	16.74	0.3	1.1
10	95510.70	16.7	0.0190	1.351	10	1.23	21.33	0.3	1.0
11	96013.59	20.6	0.0203	1.058	11	1.29	25.47	0.3	0.9
12	96032.09	24.9	0.0213	0.709	12	1.17	11.16	0.5	1.2
13	95329.97	4.4	0.0295	6.072	13	1.25	15.63	0.5	1.1
14	95440.24	9.5	0.0299	3.773	14	1.32	19.62	0.5	1.0
15	95549.82	12.2	0.0299	2.609	15	1.40	22.87	0.5	1.0
16	95559.43	16.7	0.0287	1.778	16	1.23	10.50	0.7	1.1
17	95692.66	20.6	0.0306	1.443	17	1.33	14.45	0.7	1.1
18	96249.02	24.9	0.0305	0.915	18	1.42	17.91	0.7	1.0
19	95431.99	4.5	0.0397	6.813	19	1.53	20.59	0.7	0.9
20	95156.38	9.4	0.0396	4.203	20	1.32	9.65	1.0	1.2
21	95287.67	12.3	0.0396	3.061	21	1.44	13.15	1.0	1.1
22	95616.24	16.4	0.0411	2.183	22	1.56	15.98	1.0	1.0
23	96075.93	20.7	0.0406	1.648	23	1.67	18.56	1.0	0.9
24	96365.30	25.0	0.0402	1.108					
25	95256.39	4.5	0.0711	9.279					
26	95441.82	9.4	0.0712	5.264					
27	95588.23	12.2	0.0718	4.017					
28	95746.18	16.4	0.0721	3.116					
29	96342.49	20.8	0.0724	2.410					
30	96686.02	25.1	0.0724	1.668					

4. RESULTS AND DISCUSSION

The results of a comparative analysis between the data from Torres (1992) and Aliyu *et al.* (2017) are presented in Figs. 1 and 2. This analysis focuses on correlations related to droplets' entrainment fraction, E_d, and interfacial friction factor, C_{fi}, evaluated regarding root mean square (RMS) of the relative deviations for δ_f. The rows in the heatmap graphs corresponding to the acronym CE represent the eleven correlations for E_d, including the assumption of $E_d = 0$ (CE0), according to Tab. 2. On the other hand, the columns labeled CF represent the ten distinct correlations previously discussed for C_{fi}, according to Tab. 3. Each RMS value obtained corresponds to a specific combination of these correlations, and the colormap indicates the highest RMS values (in red tones) and lowest RMS values (in blue tones).

Regarding the results obtained from Torres (1992), it is noticeable that the film thickness exhibits less variation based on the entrainment fraction. This phenomenon can be attributed to the significant role of gravity as a mechanism for droplets' deposition in stratified flows, leading to a lower entrainment fraction than in annular flows when considering the entire length of the pipe. It is also possible to notice that, against data from Torres (1992), CE10 by Karami *et al.* (2017) and CE3 by Oliemans *et al.* (1986) exhibited the lowest overall deviations. On the other hand, the assumption where E_d equals zero (CE0) shows the highest deviations. Concerning the friction factor, a better result was observed when using CF10 by Fukano and Furukawa (1998), while CF5 by Kowalski (1987) provided the worst values of deviations.

Against the Aliyu *et al.* (2017) data, the deviations obtained were predominantly higher than those observed for the Torres (1992) data. CE10 by Karami *et al.* (2017) and CE7 by Pan and Hanratty (2002b) for vertical pipes yield better results than other correlations. At the same time, the most significant deviations are observed for CE3 by Oliemans *et al.*

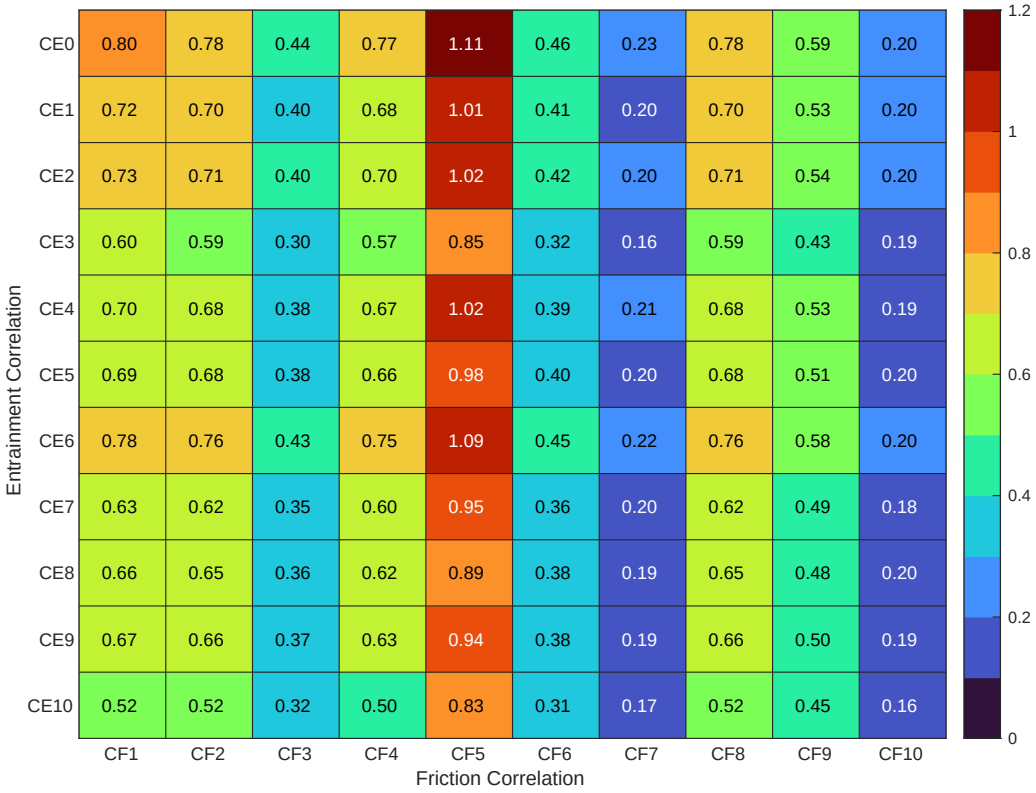

Figure 1. RMS values' heatmap of the relative deviations referent to Torres (1992) data.

Figure 2. RMS values' heatmap of the relative deviations referent to Aliyu *et al.* (2017) data.

(1986) and CE1 by Paleev and Filippovich (1966). Although CE3 was initially developed for vertical flows, it proved more effective for such flows, as Torres (1992) conducted in his experiment. The Karami *et al.* (2017) correlation, CE10, was developed for three-phase stratified flows of gas, Isopar L oil, and water, but it showed promising results compared to both datasets.

The internal diameter of the pipes in the two datasets holds significant importance. Aliyu *et al.* (2017) stated that the correlations available for predicting interfacial friction, C_{fi}, and film thickness, δ_f, generally have validity limited to a diameter range of 10 mm to 50 mm. The higher level of agreement with experimental data observed for the smaller pipe diameter of 38.1 mm, compared to the larger diameter of 101.6 mm, can be attributed to this factor. There is a noticeable disparity between the values of the dimensionless film thickness δ_f measured by the two authors since Aliyu *et al.* (2017) reported δ_f ranging from 0.007 to 0.013, whereas Torres (1992) wrote δ_f ranging from 0.013 to 0.244, corresponding to δ_f increases ranging from 86% to 1777%, approximately. Furthermore, it is evident that the correlations employed for the droplets' entrainment fraction are applicable within a narrow range of operational conditions and often exhibit inaccuracies when compared to actual results, particularly under varying conditions. The correlation's dependence on variables such as velocity and diameter must also be considered, as both parameters differ in the datasets.

5. CONCLUSIONS

This work presents a numerical model to calculate the film thickness in separated gas-liquid flows, specifically targeting horizontal stratified and vertical annular patterns. A comparative analysis was performed between the proposed models and two sets of experimental data from the literature. The evaluation criteria used for comparison were the average relative deviations and their values of the root mean square. Also, this study presents a comprehensive selection of ten correlations for the droplets' entrainment fraction and ten correlations for the interfacial friction factor, sourced from the existing literature for implementation within the numerical model. The study also conducted an in-depth analysis of the correlations' impact on fitting the experimental data.

The results demonstrated a higher level of agreement with the experimental data obtained from horizontal stratified flow (Torres, 1992) compared to vertical annular flow (Aliyu *et al.*, 2017). For stratified flow, the RMS of the relative deviations between calculated and measured film thickness was the lowest 19.5% when the droplets entrainment fraction correlation by Oliemans *et al.* (1986) was combined with the interfacial friction factor correlation by Fukano and Furukawa (1998), while the highest relative deviation 111% was obtained from the combination of the hypothesis of $E_d = 0$ and the interfacial friction factor correlation by Kowalski (1987). For annular flow, the lowest deviation was 7% when using the correlation by Oliemans *et al.* (1986) combined with the Cheremisinoff and Davis (1979) friction factor correlation. However, the highest value was obtained by the combination of Paleev and Filippovich (1966) and Kowalski (1987), which involved using a gas mixture of Freon 12 instead of pure air.

A possible explanation for the lower agreement with the annular flow data is the limited applicability of correlations to estimate the interfacial friction factor, typically restricted to internal diameter pipes ranging from 10 mm to 50 mm. In the experiments conducted by Aliyu *et al.* (2017), a pipe with a diameter of 101.6 mm was utilized, which falls outside the validity range of the correlations and could contribute to the observed disparity. Additionally, the correlations employed for estimating the droplets' entrainment fraction, influenced by various flow parameters such as the gas-liquid ratio, can contribute to deviations between calculated and measured values.

6. REFERENCES

Aliyu, A.M., Baba, Y.D., Lao, L., Yeung, H. and Chun Kim, K., 2017. "Interfacial friction in upward annular gas-liquid two-phase flow in pipes". *Experimental Thermal and Fluid Science*, Vol. 84, pp. 90–109. DOI 10.1016/j.expthermflusci.2017.02.006.

Alves, I.N., Caetano, E.F., Minami, K. and Shoham, O., 1991. "Modeling annular flow behavior for gas wells". *SPE Production Engineering*, Vol. 6, No. 4, pp. 435–440. DOI 10.2118/20384-PA.

Asali, J.C., 1984. *Entrainment in vertical gas-liquid annular flows*. Ph.D. thesis, University of Illinois at Urbana-Champaign, Champaign, IL, USA.

Bharathan, D. and Wallis, G.B., 1983. "Air-water countercurrent annular flow". *International Journal of Multiphase Flow*, Vol. 9, No. 4, pp. 349–366. DOI 10.1016/0301-9322(83)90093-9.

Cheremisinoff, N.P. and Davis, E.J., 1979. "Stratified turbulent-turbulent gas-liquid flow". *AIChE Journal*, Vol. 25, No. 1, pp. 48–56. DOI 10.1002/aic.690250106.

Fukano, T. and Furukawa, T., 1998. "Prediction of the effects of liquid viscosity on interfacial shear stress and frictional pressure drop in vertical upward gas-liquid annular flow". *International Journal of Multiphase Flow*, Vol. 24, No. 4, pp. 587–603. DOI 10.1016/s0301-9322(97)00070-0.

Fukano, T. and Ousaka, A., 1989. "Prediction of the circumferential distribution of film thickness in horizontal and near-horizontal gas-liquid annular flows". *International Journal of Multiphase Flow*, Vol. 15, No. 3, pp. 403–419. DOI 10.1016/0301-9322(89)90010-4.

Haaland, S.E., 1983. "Simple and explicit formulas for the friction factor in turbulent pipe flow". *Journal of Fluids Engineering*, Vol. 105, No. 1, pp. 89–90. DOI 10.1115/1.3240948.

Hamersma, P.J. and Hart, J., 1987. "A pressure drop correlation for gas/liquid pipe flow with a small liquid holdup". *Chemical Engineering Science*, Vol. 42, No. 5, pp. 1187–1196. DOI 10.1016/0009-2509(87)80068-4.

Ishii, M. and Mishima, K., 1989. "Droplet entrainment correlation in annular two-phase flow". *International Journal of Heat and Mass Transfer*, Vol. 32, No. 10, pp. 1835–1846. DOI 10.1016/0017-9310(89)90155-5.

Karami, H., Pereyra, E., Torres, C.F. and Sarica, C., 2017. "Droplet entrainment analysis of three-phase low liquid loading flow". *International Journal of Multiphase Flow*, Vol. 89, pp. 45–56. DOI 10.1016/j.ijmultiphaseflow.2016.10.011.

Kaya, A.S., Sarica, C. and Brill, J.P., 1999. "Comprehensive mechanistic modeling of two-phase flow in deviated wells". In *All Days*. SPE, Houston, TX, USA, pp. SPE–56522–MS. DOI 10.2118/56522-ms. Proceedings of the SPE Annual Technical Conference and Exhibition.

Kowalski, J.E., 1987. "Wall and interfacial shear stress in stratified flow in a horizontal pipe". *AIChE Journal*, Vol. 33, pp. 274–281. DOI 10.1002/aic.690330214.

Oliemans, R.V.A., Pots, B.F.M. and Trompé, N., 1986. "Modelling of annular dispersed two-phase flow in vertical pipes". *International Journal of Multiphase Flow*, Vol. 12, No. 5, pp. 711–732. DOI 10.1016/0301-9322(86)90047-9.

Owen, D.G., 1986. *An experimental and theoretical analysis of equilibrium annular flows*. Ph.D. thesis, Faculty of Science & Engineering, University of Birmingham, Birmingham, UK.

Paleev, I.I. and Filippovich, B.S., 1966. "Phenomena of liquid transfer in two-phase dispersed annular flow". *International Journal of Heat and Mass Transfer*, Vol. 9, No. 10, pp. 1089–1093. DOI 10.1016/0017-9310(66)90031-7.

Pan, L. and Hanratty, T.J., 2002a. "Correlation of entrainment for annular flow in horizontal pipes". *International Journal of Multiphase Flow*, Vol. 28, No. 3, pp. 385–408. DOI 10.1016/s0301-9322(01)00074-x.

Pan, L. and Hanratty, T.J., 2002b. "Correlation of entrainment for annular flow in vertical pipes". *International Journal of Multiphase Flow*, Vol. 28, No. 3, pp. 363–384. DOI 10.1016/s0301-9322(01)00073-8.

Pedras, M.H.J., 1993. *Atrito interfacial em escoamento anular transicional*. Master's thesis, Universidade Estadual de Campinas, Campinas, SP. DOI 10.47749/t/unicamp.1993.62352. URL `https://hdl.handle.net/20.500.12733/1580362`.

Sawant, P., Ishii, M. and Mori, M., 2008. "Droplet entrainment correlation in vertical upward co-current annular two-phase flow". *Nuclear Engineering and Design*, Vol. 238, No. 6, pp. 1342–1352. DOI 10.1016/j.nucengdes.2007.10.005.

Sawant, P., Ishii, M. and Mori, M., 2009. "Prediction of amount of entrained droplets in vertical annular two-phase flow". *International Journal of Heat and Fluid Flow*, Vol. 30, No. 4, pp. 715–728. DOI 10.1016/j.ijheatfluidflow.2009.03.003.

Seshadri, A., Mahadevan, S. and Muniyandi, V., 2014. "Measurement of liquid film thickness in air–water two phase flows in conventional and mini channels using image processing". *Korean Journal of Chemical Engineering*, Vol. 32, pp. 826–836. DOI 10.1007/s11814-014-0246-5.

Shoham, O., 2006. *Mechanistic modeling of gas-liquid two-phase flow in pipes*. Society of Petroleum Engineers (SPE).

Taitel, Y. and Dukler, A.E., 1976. "A model for predicting flow regime transitions in horizontal and near horizontal gas-liquid flow". *AIChE Journal*, Vol. 22, No. 1, pp. 47–55. DOI 10.1002/aic.690220105.

Torres, F.R., 1992. *Caracterização da interface e determinação experimental do fator de atrito interfacial em escoamento horizontais estratificados*. Master's thesis, Universidade Estadual de Campinas, Campinas, SP. DOI 10.47749/t/unicamp.1992.108039. URL `https://hdl.handle.net/20.500.12733/1583712`.

Wallis, G.B., 1968. "Phenomena of liquid transfer in two-phase dispersed annular flow". *International Journal of Heat and Mass Transfer*, Vol. 11, No. 4, pp. 783–785. DOI 10.1016/0017-9310(68)90081-1. Letters to the editors.

Whalley, P.B. and Hewitt, G.F., 1978. "The correlation of liquid entrainment fraction and entrainment rate in annular two-phase flow". Technical report, Atomic Energy Research Establishment (AERE), Harwell, Oxon, UK. Final Report: AERE-R 9187.

Xiao, J.J., Shoham, O. and Brill, J.P., 1990. "A comprehensive mechanistic model for two-phase flow in pipelines". In *All Days*. SPE, Houston, TX, USA, pp. SPE–20631–MS. DOI 10.2118/20631-MS. Proceedings of the SPE Annual Technical Conference and Exhibition.

7. RESPONSIBILITY NOTICE

The authors are solely responsible for the printed material included in this paper.